PHARMACOLOGICAL CHARACTERIZATION OF VOLTAGE- AND LIGAND-GATED ION CHANNELS BY QPatch™

sophion

SOPHION BIOSCIENCE A/S
Baltorpvej 154, DK-2750 Ballerup, DENMARK
info@sophion.dk, www.sophion.com

HERVØR LYKKE OLSEN | RASMUS B. JACOBSEN | SØREN FRIIS | RIKKE SCHRØDER | MAJ KNIRKE JENSEN | NAJA M. SØRENSEN | NIELS J. WILLUMSEN

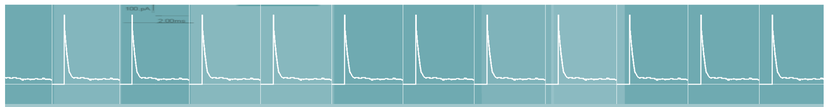

Fast and efficient characterization of drug effects on ion channels is demanded for ion channel drug discovery and development, and for safety screening. We here report pharmacological characterization of a selection of voltage- and ligand-gated ion channels obtained with the automated QPatch 16 patch-clamp system.

MATERIALS AND METHODS

Cell cultures
Cultured HEK293, CHO, RLE or RBL-2H3 cells were employed. Type of expression cell system is indicated at each figure.

Patch-clamp system.
The QPatch 16 operates 16 patch-clamp sites simultaneously and in parallel, each with an individual state-of-the-art low noise patch-clamp amplifier. It is a second generation system that can operate unattended for four hours or more, due to its on-board cell maintenance and preparation facility.
It is based on planar glass-coated silicon patch-clamp chips.
With QPatch 16 simple or complex voltage- and compound application protocols can be performed. Solution exchange time constants are in the 50-70 msec range, which is required especially for studies of some ligand-gated ion channels.

Problems with 'sticky compounds' have been minimized by the use of glass-coated surfaces throughout the microfluidic flow channel system, and by the use of teflon-coated pipettes.
Voltage- and compound application protocols are indicated in the figure legends.

Data analysis
Recorded ion channel whole-cell currents were stored in an integrated database (Oracle). Drug effects were analyzed as function of concentration (dose-response relationship). In addition, Na^+ channel inactivation kinetics (Boltzmann fits) and state-dependency were analyzed. All data analysis was accomplished with the QPatch Assay Software.

Voltage-gated potassium channels

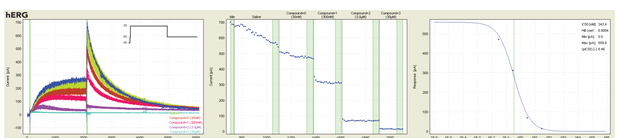

Figure 1.
Concentration-response analysis for verapamil on CHO-hERG currents. **Left** Raw current data: K^+ currents blocked by verapamil (0.03, 0.3, 3, 30 µM). V-protocol shown in inset. **Middle** I-t plot of hERG currents. **Right** Resulting Hill fit. IC_{50}=185±120 nM (n=15).

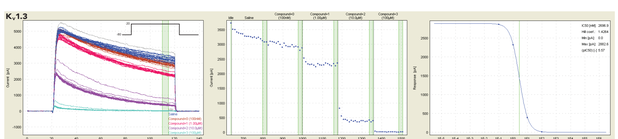

Figure 2.
Concentration-response analysis for quinidine on CHO-K_V1.3 currents. **Left** Raw current data: K^+ currents blocked by quinidine (0.1, 1, 10, 100 µM). **Middle** I-t plot of K_V1.3 current blockade. **Right** Resulting Hill fit. IC_{50}=2.44±0.29 µM (n=4).

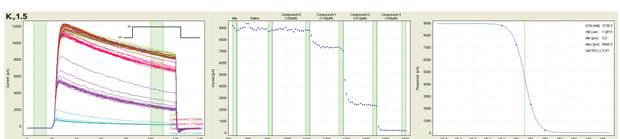

Figure 3.
Concentration-response analysis for quinidine on CHO-K_V1.5 currents. **Left** Raw current data: K^+ currents blocked by quinidine (0.1, 1, 10, 100 µM). **Middle** I-t plot of K_V1.5 current blockade. **Right** Resulting Hill fit. IC_{50}=9.7±2.0 µM (n=5).

Voltage-gated sodium channels

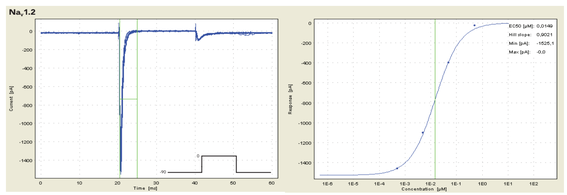

Figure 4.
Concentration-response analysis for tetrodotoxin (TTX) on HEK293-Na_V1.2 currents. **Left** Raw current data: Na^+ current blocked by TTX (0.5, 5, 50, 500 nM). **Right** Resulting Hill fit. IC_{50}=11.1±2.0 nM (n=9).

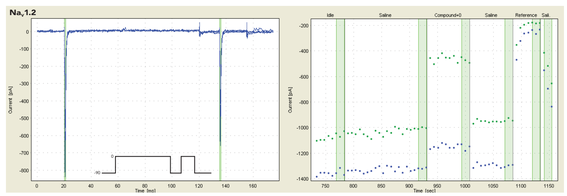

Figure 5.
State-dependency analysis of compound action on HEK293-Na_V1.2 currents. **Left** Raw current data: paired-pulse V-protocol executed during application of a state-dependent blocker (lidocaine, 100 µM), and a non-state-dependent blocker (TTX, 50 nM). **Right** I-t plot demonstrating that lidocaine predominantly affects the second peak (green), while TTX almost completely blocks the first (blue) as well as the second peak.

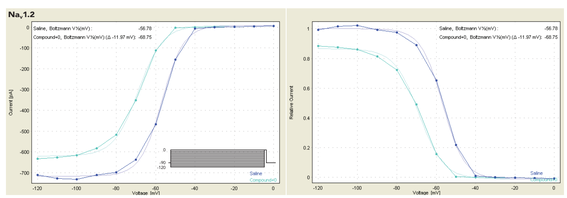

Figure 6.
Steady-state inactivation of HEK293-Na_V1.2 currents. **Left** whole-cell currents as function of the conditioning potential (see V-protocol in inset) in the absence (dark blue) and presence of 100 µM lidocaine (light blue). Data were fitted with a Boltzmann equation. Lidocaine shifted $V_{1/2}$ leftward by 12 mV. **Right** Normalized current data with Boltzmann fits.

Voltage-gated calcium channels

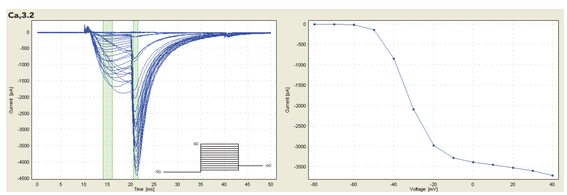

Figure 7.
I-V analysis of Ca_v3.2 expressed in HEK293 cells. **Left** raw current data: Ca^{2+} currents in response to V-protocol shown in inset. **Right** I-V relationship for the peak currents.

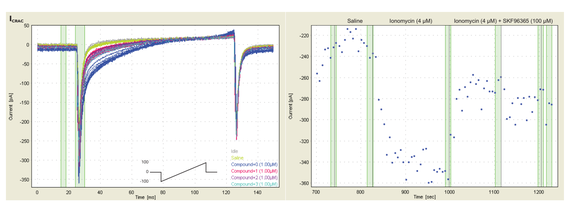

Figure 8.
Current recordings from I_{CRAC} channels expressed in RBL-2H3. **Left** Raw I_{CRAC} Ca^{2+} currents. **Right** I-t plot for the effect of 4 µM ionomycin and of ionomycin in combination with the inhibitor SKF96365 (100 µM).

Ligand-gated cation channels

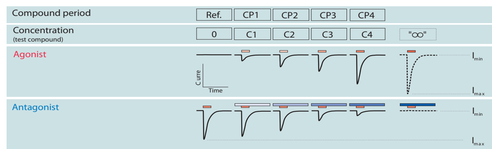

Compound application protocols
Increasing color intensities indicate increasing compound concentrations. Red color indicates agonist and blue color indicates antagonist.

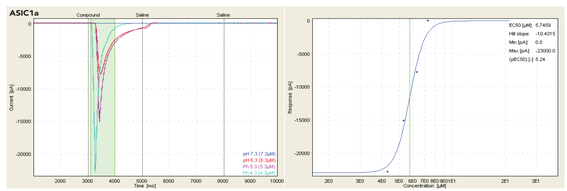

Figure 9.
Concentration-response analysis for H^+ (agonist) on HEK293-ASIC1a currents. **Left** Raw current data: ASIC1a currents obtained with increasing H^+ concentrations (pH: 7.3, 6.3, 5.3 and 4.3). V_{hold} of -90 mV. **Right** Resulting Hill fit. EC_{50}=6.3±0.3 µM (n=4).

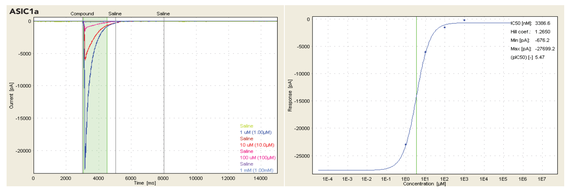

Figure 10.
Fig. 10 Concentration-response analysis for amiloride (antagonist) on HEK293-ASIC1a currents. **Left** Raw current data: ASIC1a current inhibition by amiloride at pH 4.3. **Right** Resulting Hill fit. IC_{50}=13.3±4.0 (n=4).

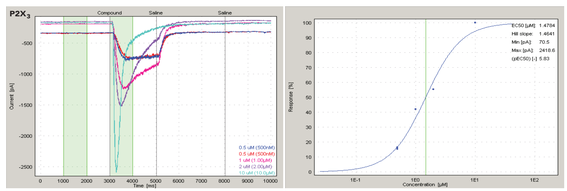

Figure 11.
Concentration-response analysis for αβ-methylene-ATP on RLE-$P2X_3$ currents. **Left** Raw current data: $P2X_3$ current traces with increasing concentrations of the agonist αβ-me-ATP (0.5, 1, 2 and 10 µM). **Right** Resulting Hill fit. EC_{50}=1.47 µM.

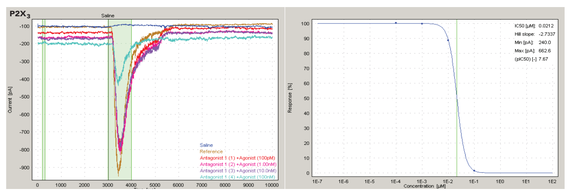

Figure 12.
Concentration-response analysis for TNP-ATP on RLE-$P2X_3$ currents. **Left** Raw current data: $P2X_3$ current inhibition by increasing concentrations of TNP-ATP (0.1, 1, 10, 100 nM) using the agonist CTP (30 µM). **Right** Resulting Hill fit. IC_{50}=21 nM.

SUMMARY

We here report pharmacological data (EC_{50} and IC_{50} values, tests for state-dependency of blockers and steady-state inactivation characteristics) from eight different types of voltage- and ligand-gated ion channels using the automated QPatch 16 system. The data obtained were in accordance with published literature values (not shown). We conclude that the QPatch technology enables fast and reliable characterization of electrophysiological ion channel properties.